First principles modeling of magnetic random access memory devices (invited)

W. H. Butler,[a] X.-G. Zhang, T. C. Schulthess, D. M. C. Nicholson, and A. B. Oparin
Metals and Ceramics Division, Oak Ridge National Laboratory, Oak Ridge, Tennessee 37831

J. M. MacLaren
Department of Physics, Tulane University, New Orleans, Louisiana 70018

Giant magnetoresistance (GMR) and spin-dependent tunneling may be used to make magnetic random access memory devices. We have applied first-principles based electronic structure techniques to understand these effects and in the case of GMR to model the transport properties of the devices. © *1999 American Institute of Physics.* [S0021-8979(99)77608-5]

I. GMR MRAM

Two approaches are currently under investigation for use as magnetic random access memory (MRAM) devices. One is based on the giant magnetoresistance (GMR) effect[1,2] with current flowing parallel to the layers. The other is based on the spin-dependent tunneling (SDT) effect[3] with the tunneling current perpendicular to the layers. Both approaches should lead to devices that are nonvolatile and resistant to ionizing radiation. In this article we will discuss the application of theoretical techniques based on first-principles electronic structure calculations to understand and improve these devices.

Figure 1 is a schematic diagram of the magnetic part of a GMR based MRAM device. Each of the layers plays an important role in the fabrication or operation of the device and each has its own set of very interesting problems. The substrate is typically an amorphous layer that has been deposited over semiconductor devices and planarized. The Ta seed layer helps to prevent damage to the semiconductor devices during the patterning of the memory cells and is also thought to promote better growth of the GMR layers. The magnetic layers should have relatively low coercivity because the ''write'' and ''sense'' currents that supply the magnetic fields that are used to switch the direction of the magnetic moments need to be kept as small as possible for efficient device operation. This need for low coercivity requires that the magnetic layers consist primarily of a material such as permalloy. The copper spacer layer is needed to break the exchange coupling between the two magnetic layers and the passivation layer is needed to prevent oxidation or corrosion of the magnetic layers.

We first consider the ''active'' part of the GMR device, the two magnetic layers and the spacer layer. The electronic structures of the nickel based alloys containing iron and cobalt as calculated within the local spin density approximation using the coherent potential approximation (CPA) have a very interesting and important feature.[4] There is very little scattering in the majority spin channel. The magnetic moment on the nickel atoms is approximately $0.6\mu_B$, the moment on the cobalt is approximately $1.6\mu_B$ and the moment on the iron is approximately $2.6\mu_B$, which means that the number of valence electrons per atom in the majority spin channel is approximately 5.3 for all three atoms. This value matches closely the 5.5 electrons per atom of copper. This near matching means that the potential scattering seen by the Fermi energy electrons is much lower in the majority channel than in the minority channel where the number of valence electrons per atom is 5.5, 4.7, 3.7 and 2.7 for copper, nickel, cobalt, and iron, respectively. The moments change only slightly near well ordered interfaces as is shown in Figures 2 and 3. These figures show the number of valence electrons per atom and spin channel as calculated[4] using the layer Korringa–Kohn–Rostoker (LKKR) technique.[5] The CPA was used to calculate the electronic structure of the permalloy ($Ni_{0.81}Fe_{0.19}$). In these calculations the moments were assumed to be collinear in the alloy, but other calculations that we have performed[6] indicate that deviations from collinearity in permalloy are small. The ''potential matching'' effect indicated here by the small changes in the number of electrons per atom in the majority spin channel is important for obtaining a large GMR.

The cobalt layer at the interface between the copper layer and the permalloy layer is beneficial in at least three ways:[7] It increases the contrast (compared to nickel) between

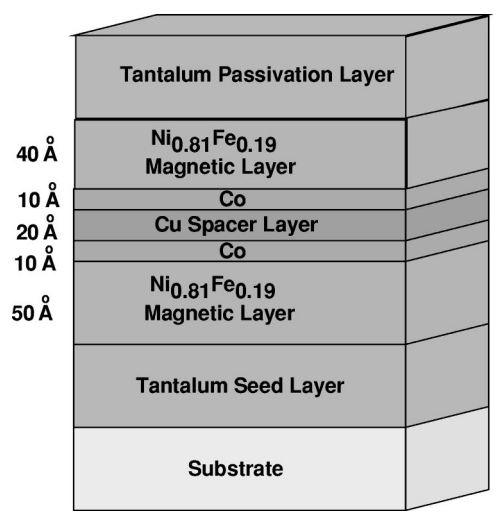

FIG. 1. Schematic of magnetic layers of an MRAM device.

[a]Electronic mail: BHB@ORNL.GOV

 © 1999 American Institute of Physics

Downloaded 12 Mar 2002 to 128.219.47.178. Redistribution subject to AIP license or copyright, see http://ojps.aip.org/japo/japcr.jsp

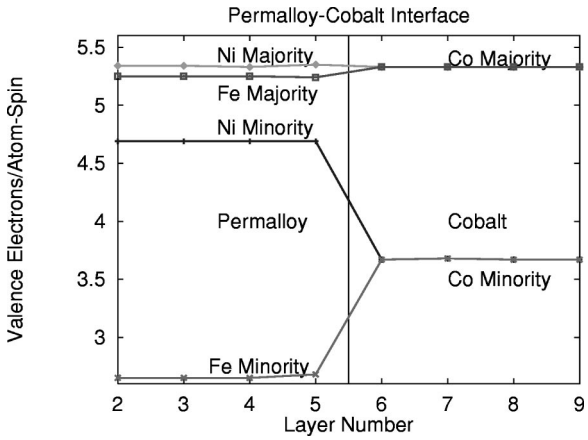

FIG. 2. Number of valence electrons per atom.

the magnetic and spacer layers in the minority channel as can be seen in Figure 4. It acts as a diffusion barrier since cobalt and copper are immiscible. Finally, it assists in maintaining exchange coupling in the magnetic layer as is illustrated in Figs. 4 and 5.

Some of the difficulties that arise when the interfaces interdiffuse are illustrated in Fig. 4 which shows the zero temperature ground state magnetic configuration of two layers of permalloy in a copper matrix after interdiffusion has occurred. The large arrows indicate the Fe moments from the permalloy. These moments are about the same size as in pure permalloy, but their directions have become disordered. These misoriented and ''loose'' moments will contribute to spin mixing and spin-flip scattering. Furthermore, the nickel moments are much smaller than for pure bulk permalloy so the majority channel does not match nearly so well to copper. When cobalt is added at the interfaces (Fig. 5) the prospects for GMR are improved significantly; the iron moments are in much better alignment and the nickel moments are closer to their bulk values. These calculations were performed using the local scalable multiple scattering approach to local spin density calculations.[8]

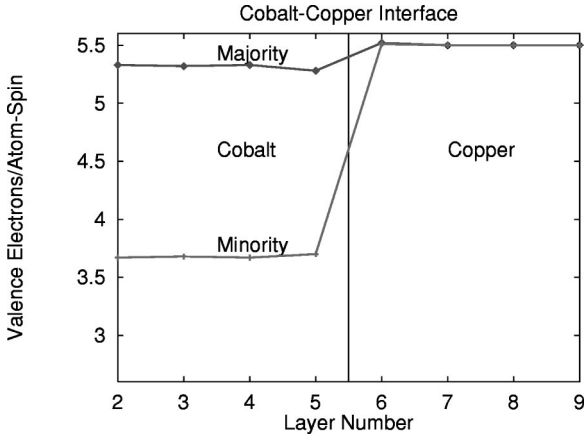

FIG. 3. Number of valence electrons per atom.

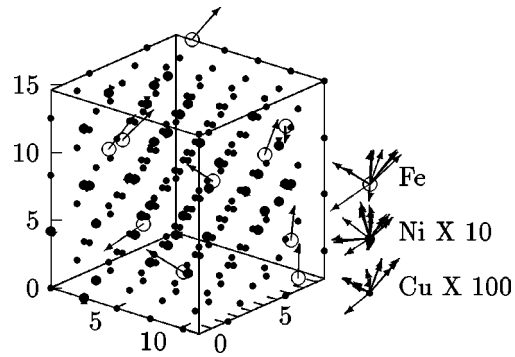

FIG. 4. Two layers of permalloy in a copper matrix. The copper and permalloy have been allowed to interdiffuse. Copper atoms are small solid circles, nickel atoms are larger solid circles, iron atoms are large open circles and have large moments indicated by arrows. The three sets of clusters of arrows to the side of the figure indicate the size of the moments and their directions for the Fe, Ni, and Cu atoms, respectively.

II. TRANSPORT MODELING

If the moments are collinear, or at least collinear within individual atomic layers, one can use specialized electronic structure techniques such as the LKKR technique to efficiently calculate the electronic structure and Green function for relatively large systems. Once the Green function is known one can calculate the nonlocal site dependent conductivity using quantum mechanical linear response theory.[9–15] Although the quantum mechanical linear response approach is very helpful in understanding the origins of the GMR, the calculations are computationally very intensive and a faster approach is needed for design and optimization of GMR based devices. It is critically important, however, to retain a reasonably accurate description of the electronic structure. We have, therefore, developed a first-principles based semiclassical approach to transport in magnetic multilayers[16] which captures most of the physics of the quantum linear response approach, but is several orders of magnitude less computationally demanding.

In this approach the effects of the electronic structure are included by using the band structure, Bloch wave velocities, and the scattering matrices characterizing the reflection and transmission of Bloch electrons at interfaces, obtained from *ab initio* electronic structure calculations using the LKKR method. These are then used in the semiclassical Boltzmann

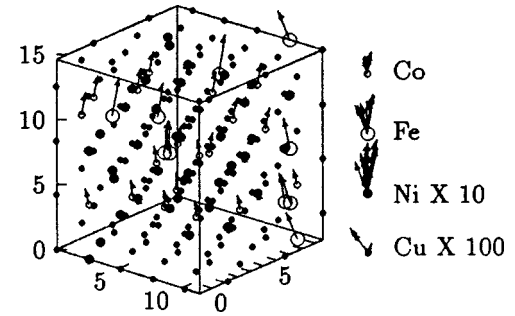

FIG. 5. Two layers of permalloy in a copper matrix with cobalt at the interface. In this case cobalt (smaller open circles with arrows) has replaced approximately one half of the copper atoms on the layers above and below the two ''permalloy'' layers. In both this and the previous figure the layer stacking used in the calculation was hcp (0001) rather than fcc(111). This should have little effect on the calculated moments.

Downloaded 12 Mar 2002 to 128.219.47.178. Redistribution subject to AIP license or copyright, see http://ojps.aip.org/japo/japcr.jsp

equation to calculate the electron current and the magnetoresistance.

The semiclassical Boltzmann transport equation (BTE) treats the electrons as classical particles that have local momentum and group velocities which are obtained from the quantum mechanical dispersion relation and which obey quantum statistics. The BTE obtains a steady state solution for the electron distribution function by considering drift, collisions, and the acceleration by the applied electric field. Since the layered system is assumed to have two-dimensional periodicity, the distribution function can be solved for each allowed parallel momentum $k_\parallel$. The distribution function is assumed to be perturbed by the presence of the applied electric field in the following manner

$$f_{i\sigma}(k_\parallel,z)=f^0_{i\sigma}(\epsilon)+\Sigma_j g^+_{ij\sigma}(k_\parallel z)+\Sigma_j g^-_{ij\sigma}(k_\parallel z), \tag{1}$$

where i refers to the layer, σ the electron spin, and the z direction is taken to be perpendicular to the layering. f^0 is the distribution function in the absence of the electric field (the Fermi–Dirac distribution) which depends upon the energy of the electron ϵ. The superscript on g indicates the direction of travel along z, or the sign of the z component of the Bloch wave group velocity v_z. Since there may be more than one Bloch state at a given $k_\parallel$ in Eq. (1), the distribution function is also labeled by a state label j.

Using the relaxation time approximation, the steady state BTE is

$$\frac{\partial g^\pm_{ij\sigma}(k_\parallel,z)}{\partial z}v^\pm_{zij\sigma}(k_\parallel)+\frac{g^\pm_{ij\sigma}(k_\parallel,z)}{\tau_{i\sigma}}=\frac{\partial f_0}{\partial\epsilon}e\mathbf{v}^\pm_{ij\sigma}\cdot\mathbf{E}, \tag{2}$$

where $\mathbf{E}$ is the electric field, e is the electronic charge, τ is the relaxation time (which also is layer and spin dependent), and $\mathbf{v}$ is the group velocity of the Bloch wave. Since each equation is labeled by the parallel wave vector $k_\parallel$ this will be assumed in all subsequent formulae. The solution to this equation is

$$g^\pm_{ij\sigma}(z)=e\tau_{i\sigma}\mathbf{v}^\pm_{ij\sigma}\cdot\mathbf{E}\frac{\partial f_0}{\partial\epsilon}(1+F^\pm_{ij\sigma}e^{\mp z/(\tau_{i\sigma}|v^\pm_{zij\sigma}|)}). \tag{3}$$

The coefficients $F^\pm_{ij\sigma}$ are found from matching the distribution function at each interface and at the two external surfaces. At the edge, $z=0$, of the first layer we have $g^+_{1\sigma}=P_l g^-_{1\sigma}$, and at the edge at $z=d$ of the last layer $g^-_{n\sigma}=P_r g^+_{n\sigma}$. P_l and P_r are the fractions of specularly scattered electrons at the left and right boundaries, respectively. Defining $T^{\pm\pm}_{i\sigma}$ as transmission and reflection matrices for an electron of spin σ at the interface between layers i and $i+1$, we have

$$g^-_{i\sigma}=S_{i\sigma}T^{-+}_{i\sigma}g^+_{i\sigma}+S_{i\sigma}T^{--}_{i\sigma}g^-_{i+1\sigma}$$
$$g^+_{i+1\sigma}=S_{i\sigma}T^{+-}_{i\sigma}g^-_{i+1\sigma}+S_{i\sigma}T^{++}_{i\sigma}g^+_{i\sigma}. \tag{4}$$

In the above the distribution functions $g^\pm$ are assumed to be vectors whose number of components equals the number of Bloch states traveling in the plus (or minus) z direction, and the terms on the right hand sides involve a matrix multiplication. The prefactors S, introduced by Hood and Falicov,[17] allow for the possibility of diffusive scattering at each interface. The fraction of the electrons that are scattered diffusively $(1-S)$ is assumed to be lost from the current carrying distribution. For the current in the plane geometry, the in-plane current density J_x is given by

$$J_{xi\sigma}=\frac{e}{(2\pi)^3}\sum_j\int d^3k[v^+_{xij\sigma}g^+_{ij\sigma}(z)+v^-_{xij\sigma}g^-_{ij\sigma}(z)]. \tag{5}$$

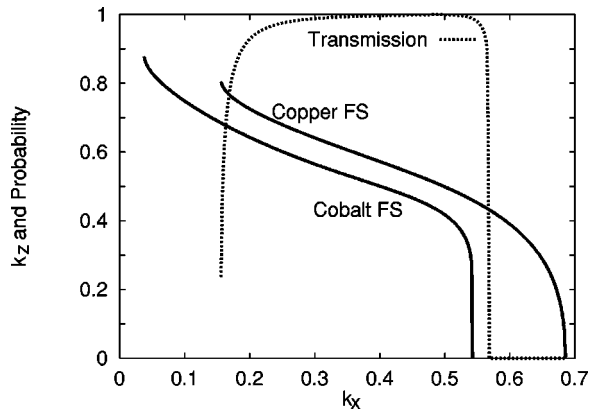

FIG. 6. Transmission probability for Bloch waves in copper incident on fcc cobalt majority as a function of $k_\parallel$ along $\bar{\Gamma}$ to $\bar{X}$.

A. Bloch wave transmission probabilities

The Bloch wave transmission and reflection matrices $T^{\pm\pm}_{i\sigma}(k_\parallel)$ depend strongly upon the electronic structure. We have devised a technique based on the Landauer formula[18] for calculating them within the layer KKR.[19] Figure 6 shows the transmission probability, (T^{++}) for Bloch waves in copper incident on majority cobalt. For values of $k_\parallel$ greater than approximately 0.57 a.u.$^{-1}$ along this direction, the transmission goes to zero because there are no states in the cobalt into which the electron waves can refract. This total internal reflection can lead to a waveguide effect that increases the GMR significantly for flat parallel interfaces. Figure 7 shows the transmission probability for Cu Bloch waves incident on minority cobalt. For both cases the interfaces are fcc (111) planes. One interesting feature of these transmission probabilities is the fact that the transmission probability goes to zero if the group velocity perpendicular to the layers of the

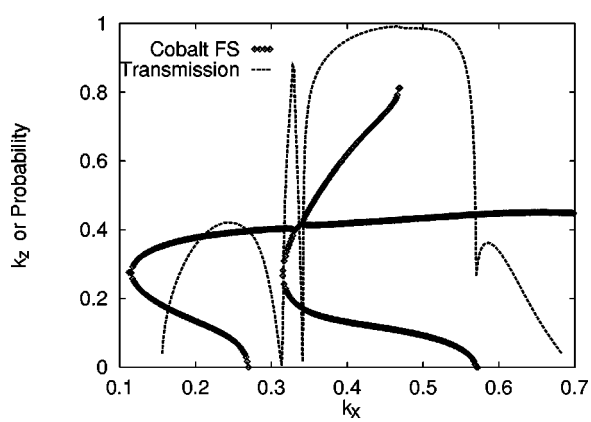

FIG. 7. Total transmission probability for Bloch waves in copper incident on fcc cobalt minority as a function of $k_\parallel$ along $\bar{\Gamma}$ to $\bar{X}$.

Downloaded 12 Mar 2002 to 128.219.47.178. Redistribution subject to AIP license or copyright, see http://ojps.aip.org/japo/japcr.jsp

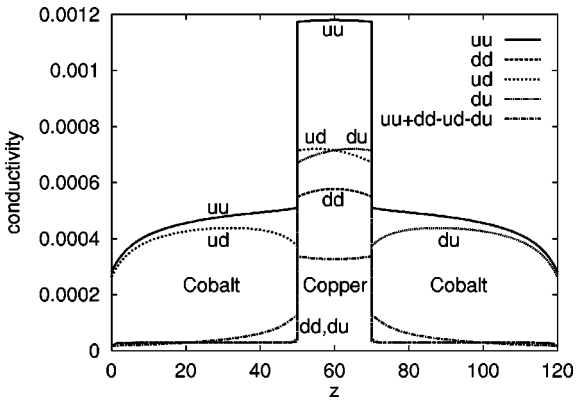

FIG. 8. Conductivity or current as a function of position in the film for the two spin channels for aligned (uu,dd) and antialigned (ud,du) moments in the two cobalt layers.

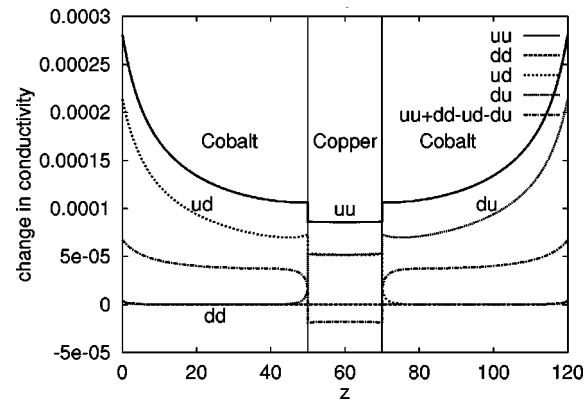

FIG. 9. Change in conductivity for each spin channel when the boundary conditions are changed from diffuse ($P=0$) to specular ($P=1$).

receiving band vanishes. This result can be derived from the fact that the electron flux must be conserved at the interfaces.

B. Effects of specular boundary scattering

We have used this approach to model spin valves used for magnetic memory applications and to evaluate the effects of changing geometry and scattering rates in the different layers. Recently we have used this approach to investigate the effects of specular scattering at the boundaries of the spin valves on the GMR. One might expect that specular scattering at the boundaries would always increase the GMR. We find that when specular boundary scattering is compared to diffuse boundary scattering, the conductance is always higher for specular scattering, for both parallel and antiparallel alignment of the moments of the two magnetic layers. Only when the majority mean free path (assuming potential matching in the majority channel) is long compared to the thickness of the magnetic layer, however, does specular boundary scattering significantly increase the GMR.

Figure 8 shows the calculated conductivity as a function of position through a Co|Cu|Co film for the case of completely diffuse boundary scattering. The scattering rate for the copper layer is such that bulk copper would have a resistivity of 3 $\mu\Omega$ cm. The scattering rates for the cobalt spin channels are chosen such that bulk cobalt would have a resistivity of 15 $\mu\Omega$ cm with the scattering rate 20 times higher in the minority channel than the majority channel. Specular scattering is assumed for the internal interfaces between the cobalt and copper layers. The calculated GMR is 14.3% for diffuse boundary scattering and increases to 16.6% for specular boundary scattering. The change in conductivity that occurs on changing the boundary scattering from diffuse ($P=0$) to specular ($P=1$) is shown in Fig. 9 where it can be seen that the contributions to this change are positive in the cobalt layers but negative in the copper layer. It is negative in the copper layer because the change from $P=0$ to $P=1$ increases the conductivity in the copper layer for both of the spin channels for the antiparallel alignment whereas only the majority channel conductivity is increased significantly in the copper for parallel alignment.

If the mean free path for the majority channel is reduced by a factor of 2, the GMR can actually increase slightly when the boundary scattering is changed from diffuse to specular. Qualitatively, this result, that the effect of specular scattering increases the GMR when the majority mean free path is long and decreases it slightly when it is sufficiently short, is grossly independent of the diffuseness of the scattering at the internal Co|Cu interfaces. The result also holds if the $P=0$ boundary condition is replaced by a a very thin strongly scattering layer.

III. SPIN-DEPENDENT TUNNELING

The spin-dependent tunneling devices that are currently under consideration for magnetic memory devices utilize an insulating layer of oxidized aluminum. This oxide is usually described as ''amorphous'' and is difficult to treat using first-principles techniques. Therefore our initial efforts are aimed at understanding the spin-dependent tunneling process in systems that are more amenable to first-principles techniques.

Recently we have investigated spin-dependent tunneling in systems of the form Fe|S|Fe where S represents an insulator or semiconductor. In particular, we have studied the semiconductors Ge, GaAs, and ZnSe which have lattices that match almost perfectly to Fe using (100) interfaces for both materials.[20,21] We find that these systems show a remarkably large magnetoresistance the microscopic origins of which can be analyzed in detail.

As the semiconducting layer is made thicker, the tunneling conductance decreases exponentially for all values of $k_{\parallel}$, but this decrease is slowest for $k_{\parallel}=0$, i.e., for those electrons whose momentum in the iron is perpendicular to the interface with the semiconductor. Figure 10 shows the density of states (DOS) for each of the bands in Fe at the Fermi energy for $k_{\parallel}=0$. It also shows how the DOS decays within the semiconductor which in this case is ZnSe. This density of states is calculated for a particular incident Bloch state on the left, all possible reflected Bloch states on the left and all possible transmitted Bloch states on the right. It can be seen that the incident Bloch states differ in how well they are *injected* into the semiconductor, their *rate of decay* within

Downloaded 12 Mar 2002 to 128.219.47.178. Redistribution subject to AIP license or copyright, see http://ojps.aip.org/japo/japcr.jsp

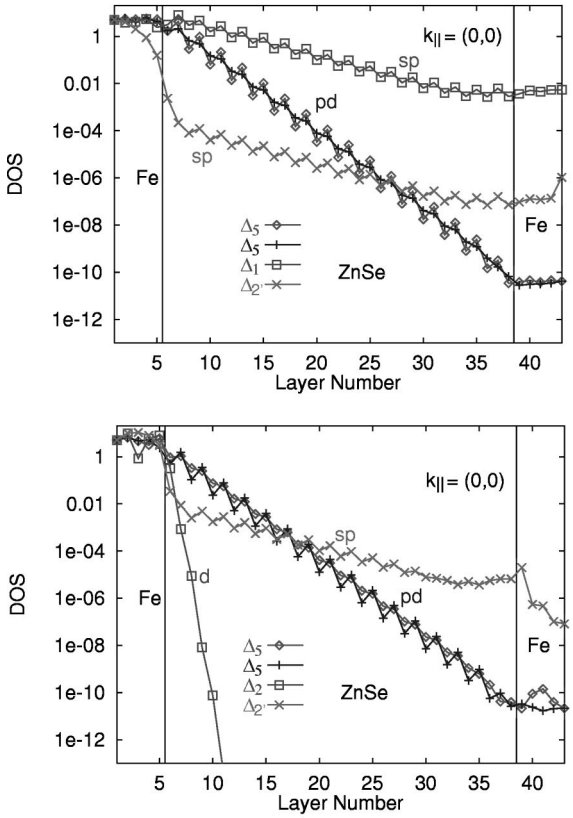

FIG. 10. Majority (upper panel) and minority (lower panel) density of states for each of the Fe Fermi energy Bloch states for $k_{\parallel}=0$. The magnetic moments on the two Fe layers are aligned parallel.

the semiconductor and how well they are *extracted* from the semiconductor to form the transmitted wave on the right.

For both majority and minority Fe for $k_{\parallel}=(0,0)$ at E_F there are four bands. A doubly degenerate Δ_5 band (compatible with p and d DOS), a $\Delta_{2'}$ band (compatible with d DOS) are found for both majority and minority. In addition, there is a majority Δ_1 band (compatible with s,p and d DOS) and a minority Δ_2 band (compatible with d DOS).

Three decay rates can be discerned within the semiconductor, one associated with the Δ_1 and Δ_2' bands, one connected with the Δ_5 bands and a very rapid decay associated with the Δ_2 band. The angular momentum composition of the DOS within the semiconductor is noted on the figure for each of the bands. It can be seen that the Δ_1 and Δ_5 bands are efficiently injected into the semiconductor on the left and extracted from it on the right. However the Δ_5 bands couple into evanescent states in the semiconductor that decay relatively rapidly within the semiconductor. The $\Delta_{2'}$ bands decay relatively slowly within the ZnSe, but are injected and extracted with very low efficiency. Only the majority Δ_1 band is both injected efficiently and decays slowly. It should be clear, because of the logarithmic scale, that for reasonably thick samples the parallel alignment conductance is dominated by the Δ_1 band and the majority spin channel.

Figure 11 shows the DOS for majority Bloch states incident from the left when the Fe moments are aligned antiparallel. The DOS is similar to the upper panel of Fig. 10

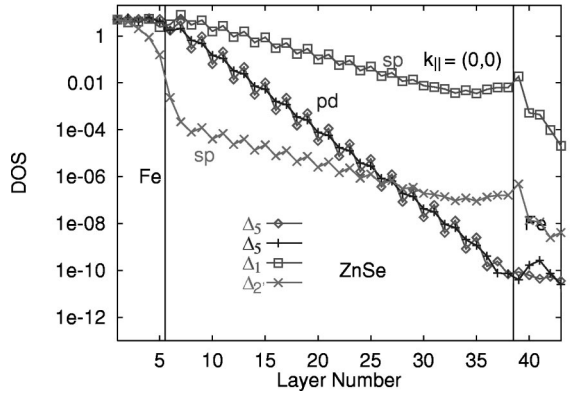

FIG. 11. DOS for each of the Fe Fermi energy Bloch states for $k_{\parallel}=0$. The magnetic moments on the two Fe layers are aligned parallel. The Fe majority Bloch states are incident from the left.

with the major difference that the Δ_1 band does not couple efficiently from the ZnSe into the minority Fe bands. Because of this poor extraction efficiency, the conductance for antiparallel alignment is much lower than for parallel alignment.

These results give insight into a very deep mystery concerning spin-dependent tunneling. Every time that it has been possible to determine which of the spin channels has the highest tunneling rate, it has been the majority channel.[22] This is true even for systems such as nickel for which the minority DOS at E_F exceeds the majority by an order of magnitude. One possible reason for this is that not all electrons tunnel equally well. For the particular states shown here it is those bands which have some s character that seem to be most efficient at tunneling. Many of the magnetic systems, e.g., nickel and cobalt have filled majority d bands. These ''strong'' magnets will clearly have more states with s character in the majority channel than in the minority channel. Fe does not have a filled majority d band, but, at least in the 100 direction, the band with s character dominates.

ACKNOWLEDGMENTS

Work at Oak Ridge was sponsored by the Division of Materials Sciences and the Laboratory Technology Research Program of the Office of Basic Energy Sciences of the US DOE under Contract No. DE-AC05-96OR22464 with Lockheed Marietta Energy Research Corp and by the Defense Advanced Projects Agency. Work at Tulane University was funded by the NSF Center for Photoinduced Processes, the Louisiana Board of Regents, and by DARPA Grant No. MDA 972-97-1-003.

[1] A. Hurst, J. Appl. Phys. (these proceedings).
[2] S. Tehrani, E. Chen, M. Durlam, J. M. Slaughter, and J. Shi, J. Appl. Phys. (these proceedings).
[3] S. S. P. Parkin, J. Appl. Phys. (these proceedings).
[4] W. H. Butler, X.-G. Zhang, D. M. C. Nicholson, and J. M. MacLaren, J. Magn. Magn. Mater. **151**, 354 (1995).
[5] J. M. MacLaren, D. D. Vvedensky, R. C. Albers, and J. B. Pendry, Comput. Phys. Commun. **60**, 365 (1990).
[6] D. M. C. Nicholson, W. H. Butler, W. A. Shelton, Y. Wang, X.-G. Zhang, and G. M. Stocks, J. Appl. Phys. **81**, 4023 (1997).
[7] D. M. C. Nicholson, W. H. Butler, X.-G. Zhang, J. M. MacLaren, B. A.

Downloaded 12 Mar 2002 to 128.219.47.178. Redistribution subject to AIP license or copyright, see http://ojps.aip.org/japo/japcr.jsp

Gurney, and V. S. Speriosu, J. Appl. Phys. **76**, 6805 (1994).
[8] Y. Wang, G. M. Stocks, W. A. Shelton, D. M. C. Nicholson, Z. Szotek, and W. M. Temmerman, Phys. Rev. Lett. **75**, 2867 (1995).
[9] W. H. Butler, X.-G. Zhang, D. M. C. Nicholson, and J. M. MacLaren, J. Appl. Phys. **76**, 6808 (1994).
[10] X.-G. Zhang and W. H. Butler, Phys. Rev. B **51**, 10085 (1995).
[11] W. H. Butler, X.-G. Zhang, D. M. C. Nicholson, and J. M. MacLaren, Mater. Res. Soc. Symp. Proc. **384**, 291 (1995).
[12] W. H. Butler, X.-G. Zhang, D. M. C. Nicholson, and J. M. MacLaren, Phys. Rev. B **52**, 13399 (1995).
[13] W. H. Butler, X.-G. Zhang, T. C. Schulthess, D. M. C. Nicholson, J. M. MacLaren, V. S. Speriosu, and B. A. Gurney, Phys. Rev. B **56**, (1997).
[14] W. H. Butler, X.-G. Zhang, D. M. C. Nicholson, T. C. Schulthess, and J. M. MacLaren, J. Appl. Phys. **79**, 5282 (1996).
[15] W. H. Butler, X.-G. Zhang, D. M. C. Nicholson, T. C. Schulthess, and J. M. MacLaren, Phys. Rev. Lett. **76**, 3216 (1996).
[16] W. H. Butler, X.-G. Zhang, and J. M. MacLaren, IEEE Trans. Magn. **34**, 927 (1998).
[17] R. Landauer, IBM J. Res. Dev. **1**, 223 (1957).
[18] J. M. MacLaren, X.-G. Zhang, X. Wang, and W.H. Butler, Phys. Rev. B (submitted).
[19] R. Q. Hood and L. M. Falicov, Phys. Rev. B **46**, 8287 (1992); L. M. Falicov and R. Q. Hood, J. Appl. Phys. **76**, 6595 (1994).
[20] W. H. Butler, X.-G. Zhang, X.-D. Wang, J. van Ek, and J. M. MacLaren, J. Appl. Phys. **81**, 5518 (1997).
[21] J. M. MacLaren, W. H. Butler, and X. G. Zhang, J. Appl. Phys. **83**, 6521 (1998).
[22] R. Meservey and P. M. Tedrow, Phys. Rep. **238**, 173 (1994).

Downloaded 12 Mar 2002 to 128.219.47.178. Redistribution subject to AIP license or copyright, see http://ojps.aip.org/japo/japcr.jsp